

Structure of latent tracks created by swift heavy-ion bombardment of amorphous SiO₂

K. Awazu*

Quantum Radiation Division, Electrotechnical Laboratory, 1-1-4 Umezono, Tsukuba 305-8568, Japan

S. Ishii and K. Shima

Tandem Accelerator Center, University of Tsukuba, Tennoudai, Tsukuba 305-8577, Japan

S. Roorda and J. L. Brebner

Groupe de Recherche en Physique et Technologie des Couches Minces (GCM), Département de Physique, Université de Montréal,

P.O. Box 6128, succursale Centre-ville, Montréal, Québec, Canada H3C 3J7

(Received 1 February 2000)

The defect structure of ion irradiation damage localized in latent tracks in amorphous SiO₂ and their role in the chemical etch rate of such tracks has been studied. A variety of light and heavy ions were used with energies ranging from 4 to 127 MeV. It was found that the frequency of the infrared absorption associated with the asymmetric stretch vibration of Si-O was significantly reduced following swift heavy-ion bombardment and that the shift correlated with the enhancement of the etching rate. In contrast, no correlation between the etching rate and either the E' center or the oxygen deficient center was observed. The IR peak shift has been related to the transition of ordinal six rings of SiO₄ tetrahedra to planar three- and four-member rings, which were generated in the latent track due to the flash heating and quenching by bombardment. We propose that large numbers of planar three- and four-member rings in the latent track are responsible for the fast chemical etching rate.

I. INTRODUCTION: LATENT TRACKS AND DEFECT CENTERS

In most insulators, the passage of swift (multi-MeV) heavy ions creates a heavily damaged, cylindrical zone known as the latent track. The majority of studies of latent tracks during the last 30 years or so were aimed at understanding the formation mechanism and a number of models have been proposed. Since the introduction rates of point defects due to nuclear collisions along the ion trajectory is far too small to explain the appearance of latent tracks, it is clear that the electronic stopping of the ions is responsible for the track formation. As a result of this electronic stopping, the wake of the ion contains a high density of energetic electrons. The proposed models differ in how, and how fast, these excited electrons transfer their energy to the atomic network. In the thermal spike model,¹⁻³ the energy is rapidly and locally thermalized, leading to short-lived but extremely high temperatures along the ion track. In the ion spike or Coulomb explosion model,^{4,5} the ion track is denuded of electrons long enough for the mutual Coulombic repulsion of neighboring atoms to occur. Hybrid models have also been proposed.^{6,7} However, all these models focus on the very early stages of track formation and give little information on the expected atomic structure of the latent tracks. Moreover, the origin and structure of the defects responsible for the enhanced etch rate of the latent tracks have not been identified. Our experimental work described in this paper attempts to improve our understanding of these latter issues by approaching the problem from a number of different angles, correlating changes in infrared absorption, electron spin resonance, and x-ray photoelectron spectroscopy with the etching enhancement in latent tracks.

Amorphous SiO₂ (hereafter a -SiO₂) has often been chosen as a target for ion implantation, as is the case in the present article, because the physical and structural properties of a -SiO₂ are well known⁸⁻¹¹ and because it is readily available at high purity. In general, microscopic defects in a -SiO₂ as introduced by ion implantation can be classified in two types: paramagnetic centers on one hand, and nonstoichiometric defects such as oxygen deficient or excess centers on the other. The E' center¹² is by far the most studied because of its ease of observation by electron spin resonance (ESR). The structure of the E' center is that of $\bullet\text{Si}=\text{O}_3$, where “ \equiv ” and “ \bullet ” denote three separate Si-O bonds and an unpaired electron, respectively. Holzenkapfer *et al.*¹³ reported that two other paramagnetic centers were induced in a -SiO₂ by ion implantation, in addition to the E' center. The structure of this new center has been proposed to be that of $\bullet\text{Si}\equiv\text{SiO}_2$, where the Si atom has one unpaired electron, two bonds to O atoms, and one bond to another Si atom. The new center can thus be classified as an oxygen deficient center. Later studies have refined and reaffirmed this conclusion.¹⁴

Typical oxygen deficient centers might be Si³⁺ (Si₂O₃), Si²⁺ (SiO), and Si⁺ (Si₂O), which can be introduced by radiation through a knock-on process of oxygen atoms.¹⁵ X-ray photoelectron spectroscopy (XPS) is the most powerful method to detect these three kinds of oxygen deficient centers. Fortunately, the binding energies and widths of Si³⁺, Si²⁺, and Si⁺ as well as Si⁴⁺ (normal SiO₂) are well known.¹⁶

Macroscopic changes of a -SiO₂ resulting from radiation have been also reported by many authors. Bates, Hendricks, and Shaffer¹⁷ reported that the densities of a -SiO₂ and α quartz increased and decreased, respectively, upon neutron irradiation and that both materials stabilized at a nearly iden-

tical density of $\sim 2.27 \text{ g/cm}^3$ after irradiation with $5 \times 10^{19} \text{ h/cm}^2$ or more. Hiraiwa, Usui, and Yagi¹⁸ reported a frequency shift of the infrared (IR) absorption peak (ω_4) induced by ion implantation. This peak is associated with the asymmetric stretching mode of an oxygen atom in the Si-O-Si inter-tetrahedral bridge. They also reported that the shift $\Delta\omega$ of the frequency saturated at around -30 cm^{-1} when the nuclear-deposited energy reached $3.4 \times 10^{23} \text{ eV/cm}^3$, which is equal to the total Si-O bonding energy (3.8 eV) in a unit volume of $\alpha\text{-SiO}_2$.

The subject of the present work is to determine the defect(s) underlying the creation of individual conic holes in $\alpha\text{-SiO}_2$. It was observed that a number of defect structures make up the latent track. We observed SiO_4 tetrahedra composed of planar three- and four-member rings, the E' center, and the oxygen deficient center in the latent tracks. We propose that the planar three- and four-member rings in latent tracks are responsible for the enhanced etching rate. Neither the E' center nor the oxygen deficient center exhibit any influence on the etching rate.

II. EXPERIMENT

Ion bombardment was performed at room temperature and at a residual pressure below $1 \times 10^{-4} \text{ Pa}$. A 6-MV tandem accelerator at the Université de Montréal was employed for irradiation with 10 MeV H^+ , 15 MeV He^+ , 2 MeV Li^+ , 4 MeV C^+ , 30 MeV Si^{6+} , and 35 MeV Se^{6+} . We also used a 12-MV tandem accelerator at the Tandem Accelerator Center of the University of Tsukuba (UTTAC) for irradiation with 120 MeV Br^{11+} , 127 MeV Br^{11+} , 98 MeV I^{12+} , and 112 MeV I^{13+} . The electronic and nuclear stopping-power data calculated with TRIM91 (Ref. 19) were shown in Figs. 1(a) and (b), respectively.

In order to avoid overlap of the individual conic holes that appear after chemical etching of latent tracks, very low ion fluences (typically $1 \times 10^7 \text{ cm}^{-2}$) are required. This was achieved by diffusing the ion beam with either a C foil or an Au foil in either forward or back-scattering geometry. Figures 2 and 3 showed the arrangement of the "flux diffusers" as they were used at the 6 and the 12 MV tandem accelerators, respectively. In Fig. 2(a) (back-scattering geometry), the incident angle of collimated 4-MeV C^+ and 30-MeV Si^{6+} beams is perpendicular to a $1\text{-}\mu\text{m}$ Au film evaporated onto a polished carbon plate. Particles scattered through 150° bombarded the sample while those scattered through -150° were simultaneously counted by a solid-state nuclear detector. An Americium source of α particles was used in place of the Au thin film as an energy standard to determine the energy of scattered ions. The energy distribution of the back-scattered ions had a maximum at 3 MeV with a full width at half maximum (FWHM) $\sim 1 \text{ MeV}$ for the 4-MeV C^+ ions and 15 MeV with a FWHM $\sim 1.8 \text{ MeV}$ for the 30-MeV Si^{6+} ions.

Figure 2(b) (forward-scattering geometry) presents the alignment for the 35-MeV Se beam. Se ions were scattered by a free-standing carbon foil of $1 \mu\text{m}$ thickness. The energy distribution of the transmitted ions has an maximum at 33 MeV. Figure 2(c) shows the photograph of $\alpha\text{-SiO}_2$ surface bombarded with Se ions at an accumulated dose $1 \times 10^{10} \text{ cm}^{-2}$ using the alignment shown in Fig. 2(b) followed by 48% hydrofluoric (HF) etching for 20 sec. The transpar-

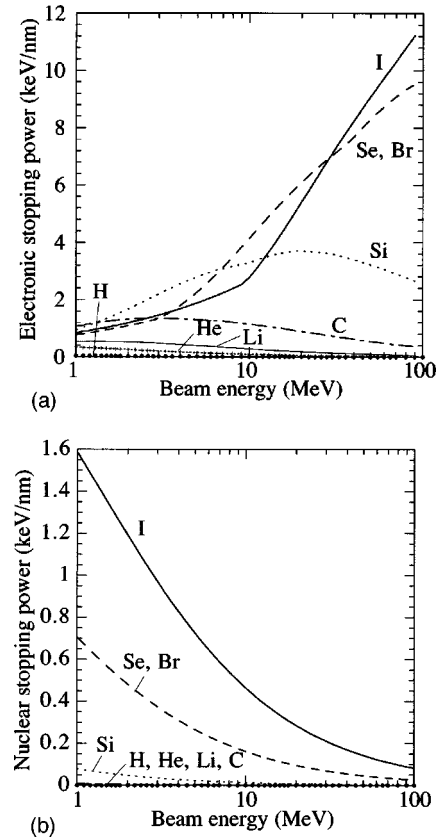


FIG. 1. (a) Electronic and (b) nuclear stopping powers vs beam energy estimated from TRIM-91.

ent circle in the center is due to relatively uniform etching, indicative of significant latent track overlap, whereas in the milky colored perimeter individual holes can be observed. The ion dose in the middle of milky colored ring amounts to $\sim 1 \times 10^7 \text{ cm}^{-2}$, as determined from counting individual etch pits visible on the photograph. Homogeneous bombardment over an area of $10 \times 10 \text{ mm}^2$ at an accumulated dose at 10^{11} cm^{-2} and higher was achieved using electrostatic x - y beam sweeping.

For 12-MV tandem accelerator, we used the other alignments shown in Figs. 3(a) and (b). A forward-scattering geometry at an angle 30° as shown in Fig. 3(a) was chosen for bombardment at a fluence of $1 \times 10^7 \text{ cm}^{-2}$. The incident energies of Br^{11+} and I^{13+} beams of 127 and 112 MeV were degraded somewhat to 92 and 76 MeV, respectively, by the passage through the 1.14-mg/cm^2 Au foil. For bombardments at fluences of $1 \times 10^{11} \text{ cm}^{-2}$ and higher, a forward-scattering geometry as shown in Fig. 3(b) was chosen. Initial beams of 120-MeV Br^{11+} and 98-MeV I^{12+} passed through Au foils of 4 and 1.14 mg/cm^2 weight, and their mean energies reduced to 67 and 80 MeV, respectively. Figure 3(c) shows the photograph of $\alpha\text{-SiO}_2$ surface bombarded with 80-MeV I ions using the alignment shown in Fig. 3(a) followed by 48% HF etching for 20 sec. The ion dose was estimated at $\sim 1 \times 10^7 \text{ cm}^{-2}$ by counting holes on a photograph.

A variety of $\alpha\text{-SiO}_2$ was used for these studies. Type III $\alpha\text{-SiO}_2$ plates of 2 mm thickness, which contain 1000 ppm OH, were used for direct observation of latent tracks. Amorphous SiO_2 films 193 nm thick were thermally grown on (100) silicon wafers in O_2 atmosphere at 1000°C . The sili-

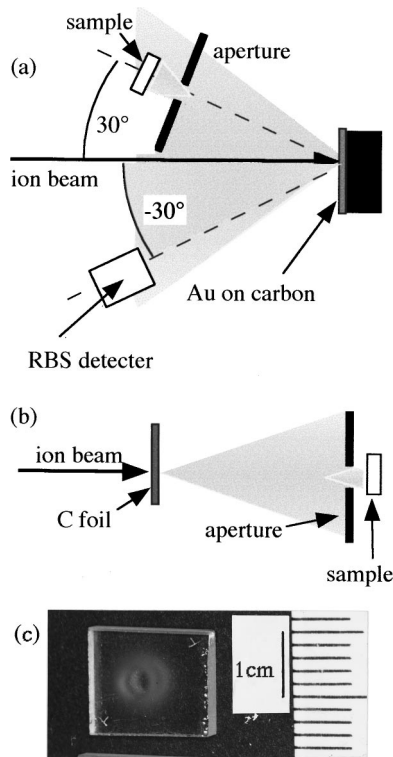


FIG. 2. Alignments of the flux diffuser installed in a beam line of 6 MV tandem accelerator in Canada. (a) Incident 4-MeV C^+ and 30-MeV Si^{6+} beams are perpendicular to a gold film $1 \mu\text{m}$ thick evaporated on a polished carbon plate to achieve an accumulated dosage $1 \times 10^7 \text{ cm}^{-2}$. Particles scattered at an angle 30° bombard the sample while the back-scattered ions were counted by a solid-state nuclear detector at an angle -30° . Energies of 4-MeV C^+ and 30-MeV Si^{6+} were reduced to 3 and 15 MeV, respectively, by scattering. (b) Alignment for the bombardment with 35-MeV Se ions at an accumulated dose $1 \times 10^7 \text{ cm}^{-2}$. Beam energy was reduced to 33 MeV by the individual carbon foil $1 \mu\text{g}/\text{cm}^2$. We could not use the alignment (a) for 35-MeV Se to avoid sputtering of an Au film on a carbon plate. (c) Amorphous SiO_2 surface bombarded with 35-MeV Se ions at an accumulated dose $1 \times 10^{10} \text{ cm}^{-2}$ followed by 48% HF etching for 20 sec, observed by optical microscope. Minimum scale in the figure presents 1 mm. Dose at the middle of milky color ring can be counted at $1 \times 10^7 \text{ cm}^{-2}$.

con wafers used in the present experiment were prepared by the floating-zone method with resistance $\sim 3000 \Omega \text{ cm}$. These wafers of $200 \mu\text{m}$ thickness were chemically polished on one side only in order to eliminate IR multiple interference effects. IR absorption was measured with a Fourier transform IR (FT-IR) spectrophotometer using light at normal incidence.

Visible individual holes were created from the irradiated samples by chemical etching with 48% hydrofluoric (HF) acid. In order to observe the cross section of holes, α - SiO_2 surfaces with holes were scratched with a diamond cutter. Cross section of the hole was observed with a scanning electron microscopy (SEM) at an angle 45° from electron incidence. X-ray photo electron spectroscopy was performed with a Vacuum Generators ESCA-3 instrument equipped with a Mg $K\alpha$ source ($h\nu = 1253.6 \text{ eV}$, linewidth $\sim 0.7 \text{ eV}$). The energy resolution of the electron analyzer was set between 0.9 and 1.20 eV.

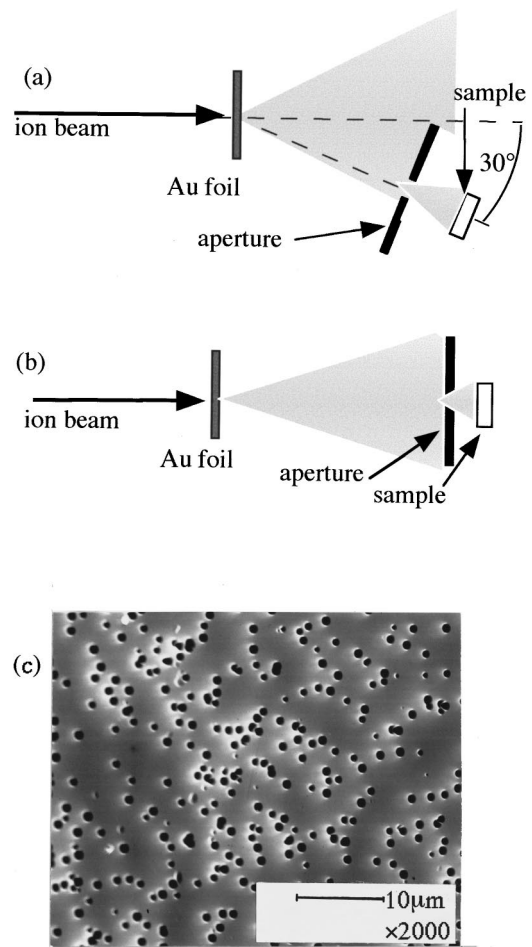


FIG. 3. Alignments of the flux diffuser installed in a beam line of 12-MV tandem accelerator in Japan. (a) Incident 127-MeV Br^{11+} and 112-MeV I^{13+} beams are perpendicular to a gold foil $1.14 \text{ mg}/\text{cm}^2$ thick to achieve an accumulated dosage $1 \times 10^7 \text{ cm}^{-2}$ at an angle 30° while beam energy was reduced to 91.7 and 76.4 MeV, respectively. (b) Alignment for the bombardment with 120-MeV Br^{11+} and 97.5-MeV I^{12+} beams to obtain accumulated doses $1 \times 10^{10} \text{ cm}^{-2}$ and higher while beam energy was reduced to 67 and 80 MeV, respectively. Au foil thickness for (a) and (b) was 2 and 4 mg/cm^2 , respectively. (c) Amorphous SiO_2 surface bombarded with 76.4-MeV I ions at an accumulated dose $1 \times 10^7 \text{ cm}^{-2}$ followed by 48% HF etching for 20 sec, observed by scanning electron microscope.

III. RESULTS

A. IR absorption spectra: Peak shifts and recovery

Figure 4 presents IR absorption spectra of a 193-nm-thick α - SiO_2 film before and after bombardment with 80-MeV I ions. The unirradiated film shows two first-order features in the IR absorption at 1078 and 805 cm^{-1} , which were labeled ω_4 and ω_3 , respectively.²⁰ Irradiation introduces a shift in opposite directions: the frequency of ω_4 decreases from 1078 to 1044 cm^{-1} whereas that of ω_3 increases from 807 to 822 cm^{-1} .

The evolution of the position of the peak labeled ω_4 for a variety of ions and as a function of ion dose is shown Fig. 5. The following ion/energy combinations are shown: 10-MeV H, 15-MeV He, 2-MeV Li, 4-MeV C, 30-MeV Si, 35-MeV Se, 67-MeV Br, and 80-MeV I. No peak shift was observed

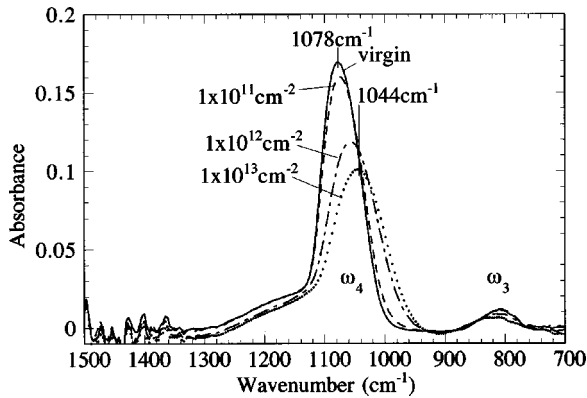


FIG. 4. IR absorption spectra of an a -SiO₂ film 193 nm thick bombarded with I ions at accumulated doses $1 \times 10^{11} \text{ cm}^{-2}$, $1 \times 10^{12} \text{ cm}^{-2}$, and $1 \times 10^{13} \text{ cm}^{-2}$. Solid line shows the spectrum of the virgin sample.

for either 10-MeV H ions or 15-MeV He ions in the dose region of 10^{16} cm^{-2} and lower. For all other ions, the frequency ω_4 decreased and saturated at 1044 cm^{-1} with increase of dose. The ion dose where saturation is reached is very different for the different ions, spanning three orders of magnitude. Otherwise, the behavior of the frequency shift as a function of ion dose is similar for all combinations with only a factor of 12–15 between the dose required to initiate a shift and that to saturate it. In order to facilitate comparison of the different ion/energy combinations, points of equal deposited energy have been identified. The open circles on each curve in Fig. 5 correspond to a deposited energy $\sim 3.4 \times 10^{23} \text{ eV/cm}^3$, which amounts to a deposited energy density approximately equal to the total Si-O bonding energy $\sim 3.8 \text{ eV}$ in a unit volume of a -SiO₂.¹⁸

Next, we examined whether thermal annealing has an effect on the IR absorption. Figure 6 shows such spectra for the same material as shown in Fig. 4, but after annealing at 600°C in He atmosphere for 10 min (dashed line), 35 min (dotted line), and 150 min (solid line). The spectra for unir-

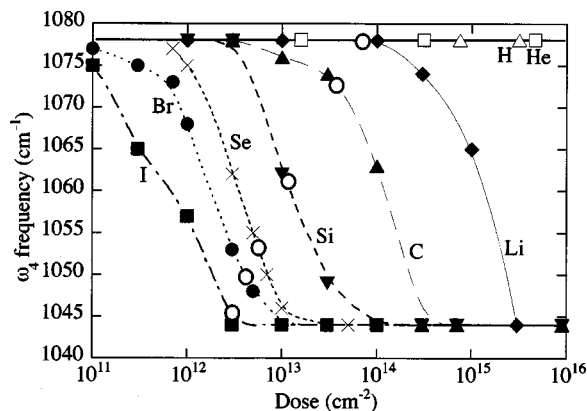


FIG. 5. Frequency at an absorption maximum of the ω_4 band against dose. 10-MeV H open squares; 15-MeV He, open triangles; 2-MeV Li, closed diamonds; 4-MeV C, closed triangles; 30-MeV Si, closed and reversed triangles; 35-MeV Se, crosses; 67-MeV Br, closed circles; 80-MeV I, closed squares. All lines are a guide for the eyes. Open circles correspond to the bond energy of Si-O which was obtained from the electronic stopping power of each ions multiplied by dose.

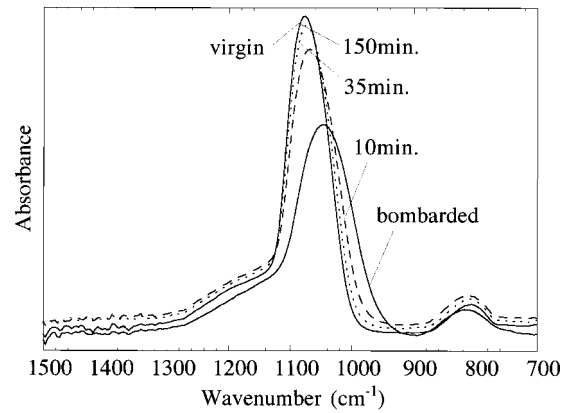


FIG. 6. IR absorption spectra of an a -SiO₂ film 193 nm thick bombarded with 80-MeV I ions at accumulated $3 \times 10^{12} \text{ cm}^{-2}$ followed by heating. Heating time at 600°C in He atmosphere is a parameter. Solid line shows the spectrum of the virgin sample.

radiated (solid line labeled “virgin”) and irradiated with $3 \times 10^{14} \text{ cm}^{-2}$ 30-MeV Si ions (solid line labeled “bombarded”) are also shown for reference. It is seen in the figure that even a short (10 min) anneal is enough to bring about a small shift of the ω_4 peak towards its original (unirradiated) position. The unirradiated and 150-min annealed spectra are essentially identical, both absorption peaks having regained their original intensities and central frequencies.

B. SEM observation: Conical holes

Some 2-mm-thick a -SiO₂ plates were irradiated followed by etching with a 48% HF solution for 20 or 45 sec. For some ion energy combinations, visible holes appeared and could be observed by SEM as shown in Fig. 6. The ion/energy combinations were: (a) 15-MeV Si, (b) 33-MeV Se, (c) and (d) 92-MeV Br, (e) 76-MeV I. The etch times were 45 sec for (a), (b), and (c) and 20 sec for (d) and (e). Some plates were scratched with a diamond point pen allowing the cross section of the holes to be observed at an angle 45° . The micrographs clearly show the conical shape of the etched holes. Observation at an angle of 45° implies that the vertical scale is different from the horizontal one on the photographs in Fig. 7. Sizes of conic holes (R , d) in nm where R and d present diameter and depth, respectively, were estimated as (a), (210, ~ 20); (b), (940, 1800); (c), (940, 1800); (d), (330, 380); (e), (530, 1900). In contrast to the heavy-ion bombardment, we could not observe any changes on a -SiO₂ plates bombarded with swift light ions 10-MeV H, 15-MeV He, 2-MeV Li, or 4-MeV C ions followed by etching with a 48% HF solution for 45 sec.

Since the modifications in the IR absorption induced by ion irradiation can be removed by thermal annealing, it was decided to investigate the effect of similar anneal treatment on the etchability of the latent tracks. Figure 8(a) shows the SEM micrographs of the same material as shown in Fig. 7(e), a 2-mm-thick a -SiO₂ plate, bombarded with $1 \times 10^{17} \text{ cm}^{-2}$, 76-MeV I and etched for 20 sec with a 48% HF solution. The mean hole diameter was estimated at 514 nm. Other such samples were annealed in He atmosphere at 400, 450, and 500°C for 150 min followed by a 20-sec etch with 48% HF. SEM micrographs of these samples, observed at an

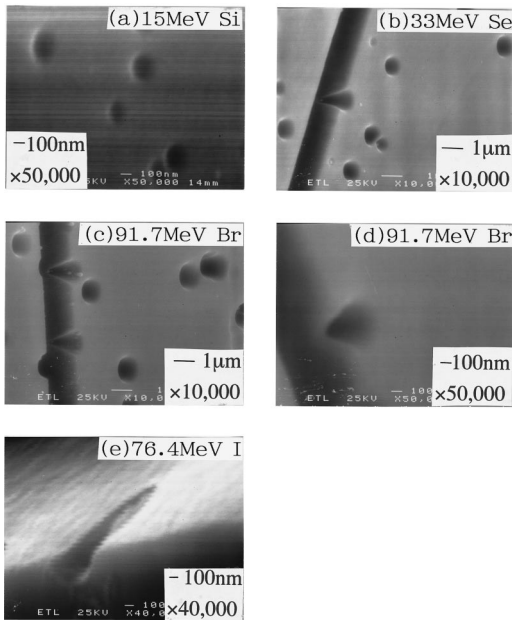


FIG. 7. SEM photographs of a -SiO₂ plates 2 mm thick bombarded with (a) 15-MeV Si, (b) 33-MeV Se, (c) and (d) 91.7-MeV Br, and (e) 76.4-MeV I ions followed by 48% HF etching for (a), (b), and (c) 45 sec and (d) and (e) 20 sec at 20 °C. All observations were performed at angle 45° to the surface. On the photographs of (b)–(e), SiO₂ surfaces were scratched with a diamond point pen to observe cross section of holes.

angle 45°, are shown in Fig. 8(b)–(d), respectively. The mean diameters were estimated at 370 ± 80 nm, 155 ± 30 nm, and 90 ± 10 nm, respectively. It appears therefore that the enhanced etchability induced by swift heavy ions is affected in a similar manner to that of the IR absorption; namely, the damage can be repaired by thermal annealing in He atmosphere.

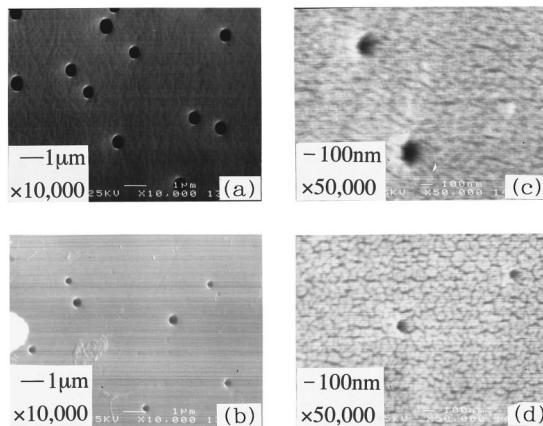


FIG. 8. SEM observation of the hole on a -SiO₂ plates 2 mm thick with heating temperature as a parameter. (a) An SiO₂ plate bombarded with 76-MeV I ions at an accumulated dose 1×10^7 cm⁻² followed by 48% HF etching for 20 sec. (b) An a -SiO₂ plate bombarded with 76-MeV I ions at accumulated dose 1×10^7 cm⁻² followed by heating at (b) 400 °C, (c) 450 °C, and (d) 500 °C for 150 min in He atmosphere. All plates were etched with a 48% HF solution for 20 sec after bombardment.

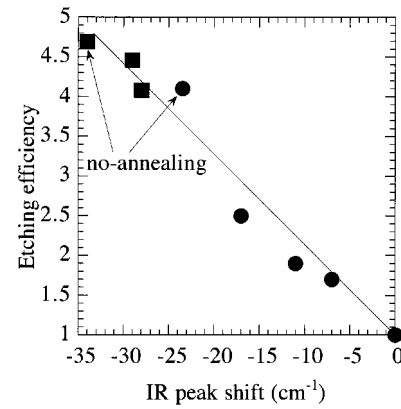


FIG. 9. Relative etching efficiency against shift of the frequency ω_4 . Amorphous SiO₂ films 193 nm thick bombarded 80-MeV I ions at accumulated doses 1×10^{12} cm⁻² (circles) and 3×10^{12} cm⁻² (squares) were annealed at 600 °C. Decrease of relative etching efficiency and increase of the frequency ω_4 were simultaneously observed with annealing. Solid line is only the guide for the eyes.

C. Simultaneous recovery of etch rate and IR peak shift

An attempt was made to quantify the correlation between the thermally induced restoration of the etch rate and the IR absorption. Instead of etching individual holes, somewhat higher ion fluences were used so that the individual tracks overlap significantly. As well, one half of the surface of a 193-nm-thick a -SiO₂ film was covered with a 0.5-mm-thick blade prior to the bombardment with 80-MeV I ions. After appropriate thermal annealing at 600 °C and etching with a diluted HF solution (48% HF: H₂O = 1:20), the step height at the border between the irradiated and the unirradiated part was measured by surface profilometry. The difference in etching rate could thus be determined from the step height divided by etching time. As well, the IR absorption was measured on the irradiated part of the samples. The results are shown in Fig. 9, which presents the relative etch rate as a function of shift of the frequency ω_4 . The etching rate and peak shifts are taken relative to unirradiated material. Therefore unirradiated a -SiO₂ gives a point in the lower right corner at (0, 1). Circles and squares denote bombarded a -SiO₂ films at accumulated doses of 1×10^{12} and 3×10^{12} cm⁻², respectively. With increasing annealing time, the relative etch rate decreases and the frequency ω_4 increases simultaneously. Both the etching rate and the ω_4 central frequency can be completely recovered to their original values by annealing at 600 °C for 150 min.

D. Paramagnetic centers

Electron spin resonance (ESR) at room temperature was used to characterize the radiation damage in 193-nm-thick, dry a -SiO₂ films. The detected signal showed g_{\parallel} and g_{\perp} values of 2.0017 and 2.0001 that have been attributed to either the E' center⁹ or to the $\bullet\text{Si}\equiv\text{SiO}_2$ center.¹³ One can distinguish between the E' center and the $\bullet\text{Si}\equiv\text{SiO}_2$ center through the saturation behavior of the signal with increasing microwave power. The intensity of the E' signal begins to saturate at a microwave power 20 μW , whereas that of the $\bullet\text{Si}\equiv\text{SiO}_2$ signal does not saturate even at 10 mW. The ESR

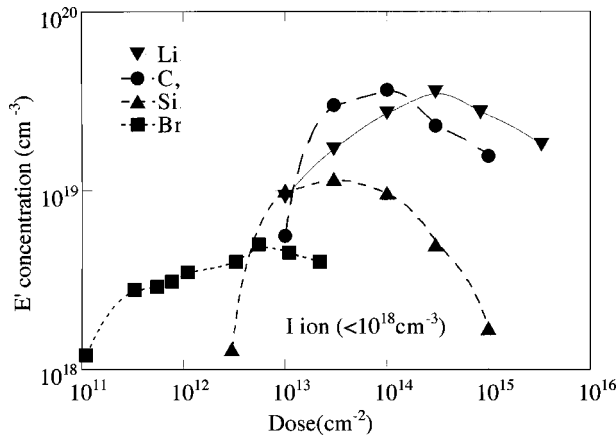


FIG. 10. Concentration of the E' center determined by ESR measurement against dose. Amorphous SiO_2 films 193 nm thick were bombarded with 2-MeV Li (reversed triangles), 4-MeV C (circles), 30-MeV Si (triangles), 67-MeV Br (squares), and 80-MeV I ions. E' center introduced by I ion bombardment was ambiguous to determine the concentration. All lines are guides for the eyes.

signals detected in our samples saturated at 20 μW and were thus attributed to the E' center.

Figure 10 shows the E' center concentration as a function of ion dose for a variety of ions, namely 2-MeV Li, 4-MeV C, 30-MeV Si, and 67-MeV Br. In all four cases, the E' density initially increases with ion dose, then reaches a maximum, and finally decreases with ion dose. The E' center concentration shows the following maximum values: For Li ions: $5 \times 10^{19} \text{ cm}^{-3}$ at $3 \times 10^{14} \text{ cm}^{-2}$; for C ions: $5 \times 10^{19} \text{ cm}^{-3}$ at $1 \times 10^{14} \text{ cm}^{-2}$; for Si ions: $1.1 \times 10^{19} \text{ cm}^{-3}$ at $3 \times 10^{13} \text{ cm}^{-2}$; and for Br ions: $6 \times 10^{18} \text{ cm}^{-3}$ at $7 \times 10^{12} \text{ cm}^{-2}$. The ESR signals in $a\text{-SiO}_2$ film bombarded with 10^{11} – 10^{15} cm^{-2} , 80-MeV I ions were ambiguous and are not shown. It is recalled here that neither the IR absorption nor the etch rate enhanced showed any maximum as a function of ion dose. It appears therefore that there is no direct correlation between the E' center density and the etch rate enhancement.

E. Oxygen deficient center

Oxygen-deficient-type defects such as the Si^{3+} structure are an important class of defects in ion bombarded $a\text{-SiO}_2$ and it should be established whether there is any correlation between these defects and the etch rate enhancement. To this end, some samples were examined with x-ray photoelectron spectroscopy (XPS). On insulating samples such as $a\text{-SiO}_2$, charge correction may be necessary and in this case, the position of the $\text{C}1s$ line from adventitious hydrocarbons (which are nearly always present) were used. Figure 11(a) illustrates a typical $\text{C}1s$ spectrum on a 193-nm-thick $a\text{-SiO}_2$ film. The spectrum can be decomposed into three peaks, i.e., a main peak and two smaller peaks which are located at binding energies 1.70 and 3.09 eV higher than the main peak energy. The ratio of the main peak to those two smaller peaks was nearly 100:10:1. This ratio was the same on all our samples and did not depend on ion species, dose, and bombardment energy. Therefore the main hydrocarbon $\text{C}1s$ peak can be used as an internal standard.

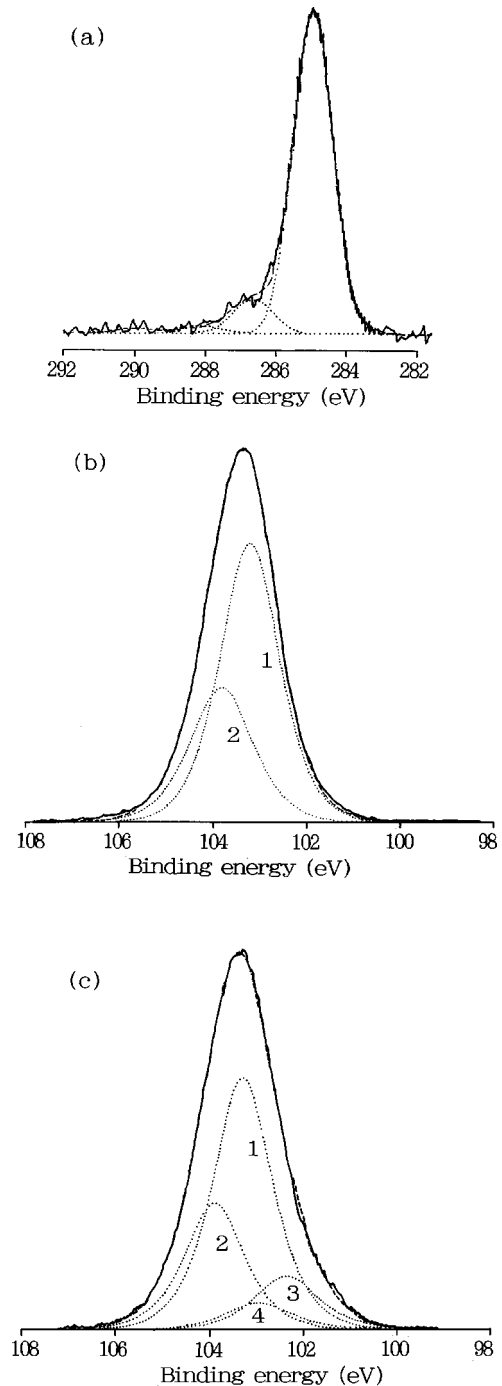


FIG. 11. XPS spectra of an $a\text{-SiO}_2$ films 193 nm thick. The largest peak in $\text{C}1s$ signal due to contamination of $a\text{-SiO}_2$ surface was used as an internal energy standard. (b) Si $2p$ signal on a virgin $a\text{-SiO}_2$ film. The signal can be divided into two signals, 1: Si $2p_{3/2}$; 2: Si $2p_{1/2}$. (c) Si $2p$ signal on an $a\text{-SiO}_2$ film bombarded with 2-MeV Li ions at an accumulated dose $3 \times 10^{14} \text{ cm}^{-2}$. 1: $\text{Si}^{4+} 2p_{3/2}$; 2: $\text{Si}^{4+} 2p_{1/2}$; 3: $\text{Si}^{3+} 2p_{3/2}$; 4: $\text{Si}^{3+} 2p_{1/2}$. Intensity ratio of the $\text{Si}^{3+} 2p_{3/2}$ and $\text{Si}^{3+} 2p_{1/2}$ is always 1:2. Parameters for decomposition were summarized in Table I.

Figure 11(b) shows the Si $2p$ spectrum of an unirradiated $a\text{-SiO}_2$ film. The spectrum can be divided into Si $2p_{1/2}$ and Si $2p_{3/2}$ spin-orbit partner lines. For a mathematically unique decomposition we used the spin-orbit splitting that have been reported and summarized in Table I.¹⁶ Intensity ratio of the Si $2p_{1/2}$ and Si $2p_{3/2}$ comes out in these fit to be equal to the

TABLE I. Parameters for decomposition of the XPS Si 2*p* spectrum.

	Si ⁴⁺ 2 <i>p</i> _{1/2}	Si ⁴⁺ 2 <i>p</i> _{3/2}	Si ³⁺ 2 <i>p</i> _{1/2}	Si ³⁺ 2 <i>p</i> _{3/2}
Peak energy (eV)	103.40	104.00	101.90	102.50
FWHM (eV)	1.50	1.50	1.45	1.45

statistical value of 1:2 within $\pm 5\%$. In the spectrum, the spin-orbit decomposed curves were shown for clarity with dotted lines. Precise peak energies of Si²⁺, Si⁺, and Si⁰ have been reported,¹⁶ yet these bonds did not need decomposition of the XPS Si 2*p* spectra of SiO₂ films bombarded with ions.

It has been also reported¹⁶ that the Si³⁺ 2*p* peak located at 1.5 eV lower than the Si⁴⁺ 2*p* peak and spin-orbit splitting of 0.60 eV is an atomic property and practically independent of the chemical environment (Table I). Figure 11(c) illustrates the analysis of the data for the Si 2*p* of an *a*-SiO₂ film bombarded with 2-MeV Li ions at an accumulated dose $3 \times 10^{14} \text{ cm}^{-2}$.

Consequently, we can write

$$x = [\text{Si}^{3+}] + 2[\text{Si}^{4+}] \quad \text{and} \quad [\text{Si}^{3+}] + [\text{Si}^{4+}] = 1 \quad (1)$$

from the intensity ratio of Si⁴⁺ 2*p* to Si³⁺ 2*p* for SiO_{*x*}. Figure 12 presents the *x* value in *a*-SiO_{*x*} obtained by bombardment of 2-MeV Li (circles), 4-MeV C (squares), 30-MeV Si (triangles), and 80-MeV I (inverted triangles) ions as a function of dose. We notice that *x* values which presents the stoichiometry do not respect the electronic stopping power shown in Fig. 1(a).

IV. DISCUSSION

A. Relationship between etching rate and shift of the frequency ω_4

The data shown in the preceding sections cover the effects of a wide range of ion species, energies, and fluences on the structure of *a*-SiO₂. To compare one ion mass with another, some scaling of the ion dose would be required. In particular, we would like to compare measurements at a fluence where the individual cylinders are just beginning to overlap. This can be estimated using an analytical formula^{20,21} for the radial profile of the spatial energy deposition. Once this radial damage profile is known, the radius *R_d* of the damage cylinder is estimated at that which contains 65% of the incident energy. From *R_d*, the minimum dose to cover the surface with damaged zone (MDDZ) was estimated with the formula

$$\text{MDDZ} (\text{cm}^{-2}) = 0.65 / \{ (10^{-7} R_d)^2 \pi \}. \quad (2)$$

TABLE II. *R_d* value is the radius of a cylinder which absorbs 65% of the incident energy. Minimum dosage to cover the surface with damaged zones (MDDZ) was estimated with the formula $\text{MDDZ} = 0.65 / \{ (10^{-7} R_d)^2 \pi \}$. Peak shifts of the frequency ω_4 at the MDDZ were estimated from Fig. 5.

	2-MeV Li	4-MeV C	30-MeV Si	35-MeV Se	78-MeV Br	78-MeV I
<i>R_d</i> (nm)	1.5	1.9	2.8	2.5	3.4	2.7
MDDZ (10^{12} cm^{-2})	9.8	8.0	6	5.5	2.7	5.1
ω_4 peak shift (cm^{-1})	0	-1	-5	-24	-25	-34
Hole diameter (a.u.)	0	0	20	92	96	145

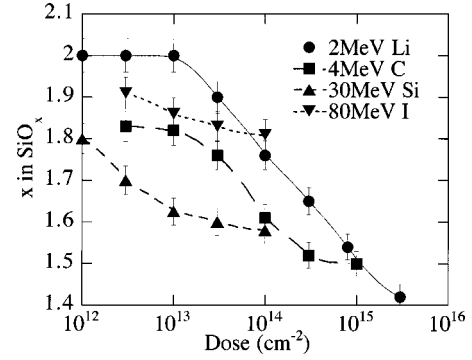


FIG. 12. The *x* value in *a*-SiO_{*x*} obtained by bombardment of 2-MeV Li (circles), 4-MeV C (squares), 30-MeV Si (triangles), and 80-MeV I (inverted triangles) ions as a function of dose. The *x* values in SiO_{*x*} were estimated from the concentration ratio of Si⁴⁺ and Si³⁺ determined from XPS Si 2*p* spectra as follows: $x = [\text{Si}^{3+}] + 2[\text{Si}^{4+}]$ and $[\text{Si}^{3+}] + [\text{Si}^{4+}] = 1$. All lines are guides for the eyes.

Values for *R_d* and MDDZ for each of the ions were summarized in Table II, as well as frequencies ω_4 at MDDZ estimated from the corresponding curves in Fig. 5. Heavy ions such as Se, Br, and I, which upon etching introduce clear individual holes on *a*-SiO₂, are seen to introduce a large shift of ω_4 at MDDZ. This would imply that even the passage of a single Se, Br, or I ion creates a latent track where the shift of the frequency ω_4 is at least -20 cm^{-1} .

Using the data from Table II, we now know which doses should be compared and thus replotted (as square symbols) as the measured diameter of etched holes against the shift of ω_4 , for all projectiles but in each case at MDDZ (Fig. 13). As well, these data are compared directly with the annealing results of 80 MeV I irradiated samples: the circles show the diameter of holes made by 80 MeV I irradiation, annealing, and etching against the shift of ω_4 . Annealing was performed prior to etching and IR absorption measurement. A maximum shift in ω_4 (at MDDZ) of -34 cm^{-1} could be obtained by bombardment with $5 \times 10^{12} \text{ cm}^{-2}$ 80 MeV I ions. An increase of ω_4 and a decrease of the hole diameter are simultaneously observed with increasing annealing temperature. Clearly, the circles (annealing) fall on the same line as the squares (different ion mass) which strongly implies that the shift of ω_4 in the latent tracks is correlated with the etching efficiency of those tracks. Moreover, these data on individual tracks complement the data shown in Fig. 9. There, we presented a correlation between the relative etch rate and the shift of ω_4 . Again, the etching efficiency is strongly correlated to the shift of the frequency ω_4 .

We now recall that open circles in Fig. 5 denote the ion

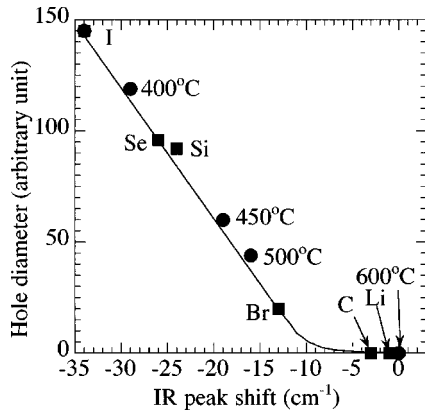


FIG. 13. Diameter of holes introduced by bombardment of 80-MeV I ions followed by etching vs shift of the frequency ω_4 at the minimum dose to cover the surface with damaged zone (MDDZ). Chemical signals for elements written near squares identified the bombarding ions. Circles present the relationship between diameter of holes introduced by bombardment of 80-MeV I ions followed by etching and shift of the frequency ω_4 at the MDDZ with the annealing temperature as a parameter. Temperatures for each experiments are presented near each plots. Solid line is guide for the eyes.

dose where the deposited energy reaches 3.4×10^{23} eV/cm³, which is approximately equal to the total Si-O bonding energy (3.8 eV) in a unit volume of *a*-SiO₂.¹⁸ The deposited energy was calculated from the electronic stopping power, multiplied by dose. The position of the open circles do not correspond with the starting point of the frequency shift of ω_4 . For example, the peak shift started when the absorbed energy exceeded the total Si-O bonding energy for 2-MeV Li ion. In contrast, the peak shift was over and saturated when the absorbed energy reached to the total Si-O bonding energy for 80-MeV I ions. This suggests that the peak shift is not related to the scission of Si-O bonds. We will discuss the scission of Si-O in the following Sec. IV C.

B. Structural model for the frequency shift

In this section we will attempt to identify a structural model for the changes in silica induced by swift heavy ions that give rise to the observed shift in ω_4 . We know that the basic building block, which is essentially a rigid entity, is the SiO₄ tetrahedron with an O-Si-O bond angle of 109.5° and these tetrahedra are placed together to construct 6–9 rings.²² Molecular orbital calculations indicate that the bond energy is minimized for an intertetrahedral, Si-O-Si bridging bond angle $\theta \sim 144^\circ$ and that for $120^\circ \leq \theta \leq 180^\circ$ there is only a weak variation in the bond energy with angle. As a good approximation, frequency of the ω_4 peak is given by

$$\omega_4 = a[2(\alpha \sin^2 \theta/2 + \beta \cos^2 \theta/2)/m]^{1/2}, \quad (3)$$

where α and β are the central and noncentral force constants, m is the mass of the oxygen atom, and θ is the bridging bond angle of Si-O-Si. If m is in Kg, and a in N m⁻¹, then the multiplying constant 5.305×10^{-12} yielding ω_4 in cm⁻¹. A compilation of data²⁵ on materials where θ has been measured directly by some method such as electron or x-ray diffraction shows that to a very good approximation, for θ

$\leq 150^\circ$, $\alpha = 582$ N m⁻¹ and $\beta = 264$ N m⁻¹. Equation (3) then enables us, with some confidence, to estimate Si-O-Si bond angles from measured IR absorption frequencies. A shift in ω_4 from 1078 cm⁻¹ to 1044 cm⁻¹ would imply a decrease in the Si-O-Si bond angle from 144° to 129°. The bond angle in a planar three member rings was estimated at 130.5°.²⁶ Therefore one candidate to explain such a strong reduction of Si-O-Si bond angle would be the reduction of ring size from six member rings to planar three and four member rings. It is interesting to compare our result on silica bombarded with swift heavy ions with that obtained on neutron irradiated amorphous silica. In that case, Raman scattering peaks D_1 at 435 cm⁻¹ and D_2 at 606 cm⁻¹, assigned to the planar four and three member rings, respectively,²⁶ were observed and the intensity of both increased with neutron bombardment. It appears that both swift heavy ions and neutral irradiation lead to the formation of planar three and four member rings and it seems reasonable that the formation mechanism would also be similar. In this context, it has been reported that both the D_1 and D_2 intensities increased with increasing ‘‘fictive temperature.’’²⁰ The ‘‘fictive temperature’’ is a higher temperature at which *a*-SiO₂ is allowed to reach an equilibrium state before a rapid quench to room temperature. According to the thermal spike model,^{1–3} the passage of a swift heavy ion introduces flash heating and quenching in amorphous SiO₂, thus creating a latent track.

C. Si-O bond scission

In Fig. 10 it was shown that concentration of E' center induced by bombardment exhibits a maximum as a function of dose. The maximum concentration was smaller for ions with a larger electronic stopping power. Moreover, there was no clear correlation between the E' concentration and the etching enhancement. For example, the largest and the deepest conic hole was observed in *a*-SiO₂ bombarded with 76-MeV I ions, but the lowest concentration was observed in those samples. Clearly, the E' center is not a good indicator for the etching efficiency of *a*-SiO₂.

Even though E' centers do not appear to play any role of significance for the etching behavior of the latent tracks, we would like to review some possible generation mechanisms of the E' center under high energy radiation. It has been reported that the E' center can be created and activated by radiation as follows:

$$[E'] \sim N_A(D) + N_C(D) = k_3[1 - \exp(-D/D_0)] + k_4D \quad (\text{Ref. 27}), \quad (4)$$

where $N_A(D)$ and $N_C(D)$ present the total number induced by activation and by creation, respectively. It has been proposed that this equation can be simplified as

$$[E'] = k_1D \quad \text{in high purity } a\text{-SiO}_2 \quad (\text{Refs. 28–30}), \quad (5)$$

or

$$[E'] = k_2D^{0.5} \quad \text{in } a\text{-SiO}_2 \text{ containing } \sim 1000 \text{ ppm OH} \quad (\text{Refs. 29 and 30}), \quad (6)$$

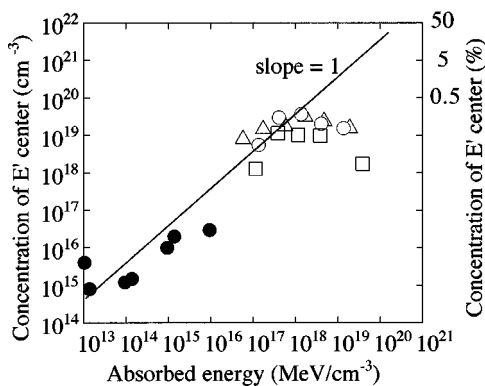


FIG. 14. Concentration of the E' center vs absorbed energy with different radiation sources. Absorption energy of gamma ray and the swift heavy ions were calculated as $AE=1.38 \times 10^8 r$ and $AE=10^4(dE_e/dx)D$, where AE , r , (dE_e/dx) , and D present the absorption energy in MeV/cm^3 , the absorption dose of gamma ray in rad (SiO_2), the electronic stopping power in keV/nm , and the accumulated dose of ion in cm^{-2} , respectively.

where D represents dose. All these equations (4)–(6) reflect the fact that normally, the E' concentration increases monotonically with IR radiation. However, we found a maximum followed by a decrease of the E' concentration. How can we explain this abnormal phenomenon?

In order to answer this question, we replotted, in Fig. 14, the E' concentration as a function of the absorbed energy with gamma-ray and ion beams. The absorption energy of the gamma-ray and ion beams were calculated as

$$AE=1.38 \times 10^8 r, \quad (7)$$

and

$$AE=10^4(dE_e/dx)D, \quad (8)$$

where AE , r , (dE_e/dx) , and D present the absorption energy in MeV/cm^3 , the absorbed dose in rad (SiO_2), the electronic stopping power in keV/nm , and the accumulated dose of ion in cm^{-2} .

The concentration of the E' center induced by gamma ray in $a\text{-SiO}_2$ films 193 nm thick obeys the rule shown in Eq. (5). If the E' center was generated according to the rule, the E' concentration would reach $\sim 10^{19} \text{ cm}^{-3}$ ($\sim 1 \text{ mol}\%$) and $\sim 10^{20} \text{ cm}^{-3}$ ($\sim 10\%$) at accumulated doses 10^{14} and 10^{15} cm^{-2} , respectively. This concentration is too high to observe all E' signals because interaction between neighboring E' centers is expected to occur. This phenomenon is now known as the “ E' - E' interaction.” One possible candidate is that the E' - E' interaction generates the oxygen deficient center, which is not a paramagnetic center, according to the following reaction:



We could not find any rule between concentration of the oxygen deficient center as detected by XPS and the electronic stopping power. For example, x values in $a\text{-SiO}_x$ at

the MDDZ $6 \times 10^{12} \text{ cm}^{-2}$ for 30 MeV Si and $5.1 \times 10^{12} \text{ cm}^{-2}$ for 80-MeV I are estimated from XPS to be 1.65 and 1.88, respectively. Nevertheless, the contour of conic holes after etching these two samples is ambiguous and clear, respectively. It should be noticed that Si ions do not directly change the stoichiometry of $a\text{-SiO}_2$ because in our experiment, all ions passed through an $a\text{-SiO}_2$ layer 193 nm thick and stopped in silicon substrate. Thus it is concluded that oxygen deficient centers detected with XPS, too, do not influence the etching efficiency of $a\text{-SiO}_2$.

We have now shown that two properties of amorphous silica indicative of Si-O bond scission, namely the E' concentration and the oxygen deficiency, do not correlate with the etching enhancement, but that there is a correlation between etching and the shift of the IR absorption ω_4 band. A complication arises now, because the ω_4 band itself is not necessarily independent of Si-O bond scission. As shown in Fig. 4, the intensity of the ω_4 band decreased with increasing accumulated dose. In a previous report,³¹ this reduction had been explained by bond scission of Si-O. Many reports have also indicated that ω_4 was strongly influenced by, for example, thickness,^{32–36} strain,³⁷ and stoichiometry.³⁸ Recently, we performed more than 80 measurements on $a\text{-SiO}_2$ films fabricated by several methods to determine the relation between the oscillator strength of ω_4 and the frequency at the absorption maximum of ω_4 .³⁹ It was found that the oscillator strength of ω_4 decreased according to the decrease in frequency in the region of $1078\text{--}1064 \text{ cm}^{-1}$, for example, in $f \sim 4.1$ at 1078 cm^{-1} and $f \sim 0.9$ at 1062 cm^{-1} . In light of the new results, it is suggested that the decrease of intensity of the ω_4 band is not attributed to scission of the Si-O bond at least in the region of $1078\text{--}1064 \text{ cm}^{-1}$.

V. SUMMARY

In summary, the defect structure of ion tracks in $a\text{-SiO}_2$ created by swift heavy ions has been studied by IR absorption, XPS, and ESR. These techniques showed how the ring statistics and the number of bond scissions changed with ion dose, and that these two phenomena behaved differently. The ion dose dependence of the etching rate enhancement correlated with the changes in ring statistics but not with bond scission or oxygen deficiency. It is concluded, therefore, that the major reason for the fast etch rate in the latent track is the generation of planar three- and four-member rings. These planar three- and four-member rings are likely introduced by a process of flash heating and quenching following the passage of a swift heavy ion.

ACKNOWLEDGMENTS

It is a pleasure to acknowledge the expert assistance of P. Bérichon and R. Gosselin with the operation of the 6-MV tandem accelerator in Université de Montréal, S. Poulin in the École Polytechnique de Montréal for XPS measurement, and A. Negishi in the Electrotechnical Laboratory for SEM observation. This work was financially supported by the Natural Science and Engineering Research Council of Canada (NSERC) and the Fonds pour la Formation de Chercheurs et l'Aide à la Recherche (FCAR).

- *Corresponding author. Present address: Quantum Radiation Division, Electrotechnical Laboratory, 1-1-4 Umezono, Tsukuba 305-8568, Japan. FAX: +81-298-61-5657. Electronic address: awazu@etl.go.jp
- ¹G. Bonfiglioli, A. Ferro, and A. Monjoni, *J. Appl. Phys.* **32**, 2499 (1961).
- ²A. Meftah, F. Brisard, J. M. Costantini, E. Dooryhee, M. Hage-Ali, M. Hervieu, J. P. Stoquert, F. Studen, and M. Toulemonde, *Phys. Rev. B* **49**, 12 457 (1994).
- ³M. Toulemonde, J. M. Costantini, Ch. Dufour, A. Meftah, E. Paumier, and F. Studer, *Nucl. Instrum. Methods Phys. Res. B* **116**, 37 (1996).
- ⁴R. L. Fleischer, *MRS Bull.* **20**, 17 (1995).
- ⁵R. L. Fleischer, P. B. Price, and R. M. Walker, *Nuclear Tracks in Solids—Principles & Applications* (University of California Press, Berkeley, 1975).
- ⁶E. Dartyge and P. Sigmund, *Phys. Rev. B* **32**, 5429 (1985).
- ⁷K. Tanimura and N. Itho, *Phys. Rev. B* **46**, 14 362 (1992).
- ⁸G. W. Arnold, *J. Non-Cryst. Solids* **179**, 288 (1994).
- ⁹R. A. Weeks, *J. Non-Cryst. Solids* **179**, 1 (1994).
- ¹⁰D. L. Griscom, *J. Ceram. Soc. Jpn.* **99**, 899 (1991).
- ¹¹R. A. B. Devine, *Nucl. Instrum. Methods Phys. Res. B* **91**, 378 (1994).
- ¹²R. A. Weeks, *J. Appl. Phys.* **27**, 1376 (1956).
- ¹³E. Holzenkämpfer, F. W. Richter, J. Stuke, and U. Voget-Grote, *J. Non-Cryst. Solids* **32**, 327 (1979).
- ¹⁴H. Hosono, H. Kawazoe, K. Oyoshi, and S. Tanaka, *J. Non-Cryst. Solids* **179**, 75 (1994).
- ¹⁵P. Mazzoldi, A. Carnera, F. Caccavale, M. L. Favaro, A. Boscolo-Boscoletto, G. Granozzi, R. Bertinello, and G. Battaglin, *J. Appl. Phys.* **70**, 3528 (1991).
- ¹⁶F. J. Himpsel, F. R. McFeely, A. Talb-Ibrahimi, J. A. Yrmoff, and G. Hollinger, *Phys. Rev. B* **38**, 6084 (1988).
- ¹⁷J. B. Bates, R. W. Hendricks, and L. B. Shaffer, *J. Chem. Phys.* **61**, 4163 (1974).
- ¹⁸A. Hiraiwa, H. Usui, and K. Yagi, *Appl. Phys. Lett.* **54**, 1106 (1989).
- ¹⁹W. Eckstein, *Computer Simulation of Ion-Solid Interactions* (Springer-Verlag, Berlin, 1991).
- ²⁰A. E. Geissberger and F. L. Galeener, *Phys. Rev. B* **28**, 3266 (1983).
- ²¹M. P. R. Waligorski, R. N. Hamm, and R. Katz, *Nucl. Tracks Radiat. Meas.* **11**, 309 (1986).
- ²²C. E. Jesurum, V. Pulim, and L. W. Hobbs, *Nucl. Instrum. Methods Phys. Res. B* **141**, 25 (1998).
- ²³P. N. Sen and M. F. Thorpe, *Phys. Rev. B* **15**, 4030 (1977).
- ²⁴A. Lehmann, L. Schumann, and K. Hübner, *Phys. Status Solidi B* **117**, 689 (1983).
- ²⁵R. A. B. Devine, *J. Non-Cryst. Solids* **152**, 50 (1993).
- ²⁶F. L. Galeener, *Solid State Commun.* **44**, 1037 (1982).
- ²⁷F. L. Galeener, D. B. Kerwin, A. J. Miller, and J. C. Mikkelsen, Jr., *Phys. Rev. B* **47**, 7760 (1993).
- ²⁸K. Awazu, H. Kawazoe, K. Harada, K. Kido, and S. Inoue, *J. Appl. Phys.* **73**, 1644 (1993).
- ²⁹K. Awazu and K. Watanabe, *Nucl. Instrum. Methods Phys. Res. B* **91**, 422 (1994).
- ³⁰H. Imai, K. Arai, J. Isoya, H. Hosono, Y. Abe, and H. Imagawa, *Phys. Rev. B* **48**, 3116 (1993).
- ³¹B. Garrido, J. Samitier, S. Bota, J. A. Moreno, J. Montserrat, and J. R. Morante, *J. Appl. Phys.* **81**, 126 (1997).
- ³²K. Sato and M. Shibata, *J. Phys. Soc. Jpn.* **21**, 1088 (1966).
- ³³H. R. Philipp, *J. Appl. Phys.* **50**, 1053 (1979).
- ³⁴M. K. Gunde and B. Aleksandrov, *Appl. Spectrosc.* **44**, 970 (1990).
- ³⁵R. Ossicovski, B. Drévilion, and M. Firon, *J. Opt. Soc. Am. A* **12**, 1797 (1995).
- ³⁶I. W. Boyd and J. I. B. Wilson, *Appl. Phys. Lett.* **50**, 320 (1987).
- ³⁷G. Lucovsky, J. T. Fitch, D. V. Tsu, and S. S. Kim, *J. Vac. Sci. Technol. A* **7**, 1136 (1989).
- ³⁸P. G. Pai, S. S. Chao, Y. Takagi, and G. Lucovsky, *J. Vac. Sci. Technol. A* **4**, 689 (1989).
- ³⁹K. Awazu, *J. Non-Cryst. Solids* **260**, 242 (1999).